

Article

# Thermal Properties and Non-Isothermal Crystallization Kinetics of Poly ( $\delta$ -Valerolactone) and Poly ( $\delta$ -Valerolactone)/Titanium Dioxide Nanocomposites

Waseem Sharaf Saeed <sup>1,\*</sup>, Abdel-Basit Al-Odayni <sup>1</sup>, Abdulaziz Ali Alghamdi <sup>1</sup>, Ali Alrahlah <sup>2,3</sup>  and Taieb Aouak <sup>1,\*</sup>

<sup>1</sup> Chemistry Department, College of Science, King Saud University, P.O. Box 2455, Riyadh 11451, Saudi Arabia; aalodayni@ksu.edu.sa (A.-B.A.-O.); aalghamdia@ksu.edu.sa (A.A.A.)

<sup>2</sup> Restorative Dental Sciences Department, College of Dentistry, King Saud University, Riyadh 11545, Saudi Arabia; aalrahlah@ksu.edu.sa

<sup>3</sup> Engineer Abdullah Bugshan research chair for Dental and Oral Rehabilitation, College of Dentistry, King Saud University, Riyadh 11545, Saudi Arabia

\* Correspondence: wsaeed@ksu.edu.sa (W.S.S.); taouak@ksu.edu.sa (T.A.); Tel.: +966-597778434 (W.S.S.); +966-563501761 (T.A.)

Received: 4 November 2018; Accepted: 3 December 2018; Published: 5 December 2018



**Abstract:** New poly ( $\delta$ -valerolactone)/titanium dioxide (PDVL/TiO<sub>2</sub>) nanocomposites with different TiO<sub>2</sub> nanoparticle loadings were prepared by the solvent-casting method and characterized by Fourier transform infra-red, differential scanning calorimetry, X-ray diffraction and scanning electron microscopy, and thermogravimetry analyses. The results obtained reveal good dispersion of TiO<sub>2</sub> nanoparticles in the polymer matrix and non-formation of new crystalline structures indicating the stability of the crystallinity of TiO<sub>2</sub> in the composite. A significant increase in the degree of crystallinity was observed with increasing TiO<sub>2</sub> content. The non-isothermal crystallization kinetics of the PDVL/TiO<sub>2</sub> system indicate that the crystallization process involves the simultaneous occurrence of two- and three-dimensional spherulitic growths. The thermal degradation analysis of this nanocomposite reveals a significant improvement in the thermal stability with increasing TiO<sub>2</sub> loading.

**Keywords:** poly( $\delta$ -valerolactone)/titanium dioxide nanocomposite; preparation; thermal behavior; non-isothermal crystallization kinetics; thermal stability

## 1. Introduction

Poly ( $\delta$ -valerolactone) (PDVL), which is a member of the poly (lactone) family, has attracted very little attention from investigators, notably in biomedical domain, compared to poly ( $\delta$ -caprolactone) PCL, even though their chemical and biomedical properties are practically similar. This semi-crystalline polyester is characterized by a lower melting point (58 °C), lower glass transition temperature (−63 °C), lower crystallization temperature, lower crystallization rate, and lower elastomeric behavior compared to PCL. These characteristics make it difficult to solidify PDVL from its melt state. This property is a key element in fusion processes, such as spinning in industrial production [1]. In addition, the lower thermal stability of PDVL, and its lower mechanical strength, reduced gas permeability, reduced solvent resistance, reduced hydrophobicity, and slower rate of degradation compared to those of the polylactone family, considerably limit its application in different fields [2]. This polymer, with five methylene groups per monomeric unit, is usually synthesized through the ring-opening

polymerization route of  $\delta$ -valerolactone using different catalytic systems [3–7]. However, because of the toxicity of some of these compounds, such as the organometallic catalysts, they are not tolerated in medical applications. The advantages that characterize this polymer with good biocompatibility, biodegradability, and permeability allow it to be used as a hydrophobic block in the amphiphilic block copolymers recommended for the construction of micellar delivery systems of hydrophobic antitumor drugs [8].

Titanium dioxide ( $\text{TiO}_2$ ), which is usually prepared from different ores, exists in three principal phases—rutile, anatase, and brookite [9]. The rutile phase is stable at high temperatures [10], and the titania phase is principally used in pigments, adsorbents, catalyst supports, filters, coatings, photoconductors, and dielectric materials.

Recently, this metal oxide has been the subject of several research studies because of its excellent electrical and photocatalytic properties.  $\text{TiO}_2$  has proven to be very useful for environmental protection applications, such as environmental cleaning, carbonic acid decomposition, and hydrogen generation [11].

The size of the  $\text{TiO}_2$  particles is considered a key factor affecting its performance, notably when mixed with a polymer as a composite material. Indeed, several researchers have focused their investigations upon the reduction of the size of  $\text{TiO}_2$  particles using different methods, such as the sol-gel technique [12–16], homogenization followed by precipitation [17], hydrothermal [18], flame synthesis [19], relatively new molten salts [20], and mechanomechanical [21,22].

These different methods were often found to produce varying results, and sometimes the same method led to particles with different sizes when a different starting material was used [23].

The synergistic combinations of polymeric materials and metal oxides through a sol-gel process have been the subject of several investigations in material science and engineering, caused by its manipulation in the molecular level leading to the development of new materials having desired and controllable properties (flexibility, hardness, durability, thermal stability, toughness, and ease of processing) [24–38]. Combining polymers with ceramics consists of a dominant polymeric phase called polymer matrix, and an inorganic ceramic phase called filler.

Combining PDVL as the polymeric phase with  $\text{TiO}_2$  as the inorganic nanofiller has at this time not been studied. The crystalline microstructure, thermal properties, and mechanical properties of the hybrid material containing a polymer and  $\text{TiO}_2$  depend mainly on the polymer/ $\text{TiO}_2$  ratio, the particle size of the  $\text{TiO}_2$  phase, dispersion of the particles in the polymer matrix, and also on interfacial forces between the two components. Indeed, the investigation carried out by Zhang et al. [39] on the poly (phenylenevinylene)/titanium oxide (PPV/ $\text{TiO}_2$ ) nanocomposite showed that the optical properties of this hybrid nanomaterial also depended on the structure of the interface between the  $\text{TiO}_2$  nanoparticles and PPV matrix.

In this same way, Kamal et al. [40] investigated the same metal oxide combined with PCL in a hybrid material fiber for use in the biomedical domain. The results obtained were that the smaller particles of the anatase phase exhibited significant enhancement of an important number of properties compared with that prepared by the rutile phase. These authors also reported that the better interactions between  $\text{TiO}_2$  anatase nanoparticles and the polymer chain drive better biocompatibility and mechanical properties.

In this work, our particular attention is focused on the investigation of some important thermal and crystallographic properties of pure PDVL and the PDVL/ $\text{TiO}_2$  nanocomposite. This system is selected to better understand the physico-chemical properties of the hybrid material for its potential use in biomedical applications, and particularly in tissue engineering.

To reach this goal, PDVL/ $\text{TiO}_2$  nanocomposite systems containing different amounts of  $\text{TiO}_2$  were prepared by the solvent-casting route, and characterized by X-ray diffraction, Fourier transform infra-red (FTIR), scanning electron microscopy (SEM), differential scanning calorimetry (DSC), and thermogravimetry analysis (TGA). Non-isothermal crystallization kinetics was chosen in this work to investigate the crystallization kinetics of PDVL and the prepared PDVL/ $\text{TiO}_2$  hybrid material,

because of compatibility with the different industrial treatment practices compared to that of isothermal crystallization kinetics. This technique can also offer great potential in the rapid processing of industrial production.

## 2. Experimental

### 2.1. Chemicals

$\delta$ -valerolactone (DVL) (purity > 99.9%), TiO<sub>2</sub> nano-powder (purity 99.7%, 21 nm primary particle size), tetrahydrofuran (THF) (purity > 99.9%), and hexane (purity 99.5%) were provided by Sigma Aldrich and used without further purification.

### 2.2. Synthesis of Poly ( $\delta$ -Valerolactone)

DVL (10 mL,  $9.64 \times 10^{-2}$  mol) was polymerized via a ring-opening reaction in the presence of 0.5 mL of hydrochloric acid (HCl) at 40 °C under nitrogen gas. A highly viscous solution was obtained at the end of the reaction, indicating the formation of PDVL. The reaction was then quenched by pouring this solution into hexane, after which white beads of PDVL were obtained. The polymer obtained was dissolved in THF and then precipitated in hexane. The PDVL obtained was then kept at 40 °C in a vacuum oven for complete drying until a constant mass was obtained. The average molecular mass and the polymolecularity index of the synthesized PDVL was determined by size exclusion chromatography (SEC) at 30 °C in THF using a Varian apparatus equipped with a JASCO, type 880-PU HPLC pump (JASCO, Easton, MD, USA), UV detectors, refractive index, and TSK Gel columns. This apparatus was calibrated with polystyrene standards, the average number molecular mass obtained was  $3.7 \times 10^4$  g·mol<sup>-1</sup>, and the polydispersity index was 3.22.

### 2.3. Preparation of PDVL/TiO<sub>2</sub> Nanocomposite

First, 0.5 g of PDVL was dissolved in THF at 80 °C under continuous stirring until complete dissolution of the polymer. A known amount of TiO<sub>2</sub> nanoparticles was added to the polymer solution under vigorous stirring for 30 h and then sonicated for 20 min to prevent agglomeration of the nanoparticles. The final PDVL/TiO<sub>2</sub> suspension was then cast in a Teflon Petri dish, air bubbles were removed by shaking and blowing air, and it was dried at ambient temperature for 24 h followed by 24 h at 50 °C in a vacuum oven to completely remove the solvent traces. A series of PDVL/TiO<sub>2</sub> nanocomposites containing 1, 2, 3, 4, and 5 wt % TiO<sub>2</sub> content were prepared by the same procedure under the conditions summarized in Table 1.

**Table 1.** Preparation conditions of poly( $\delta$ -valerolactone) (PDVL)/TiO<sub>2</sub> nanocomposites.

System	TiO <sub>2</sub> (g)	PDVL (g)	TiO <sub>2</sub> (wt %)
PDVL/TiO <sub>2</sub> -1	0.005	0.495	1.0
PDVL/TiO <sub>2</sub> -2	0.010	0.490	2.0
PDVL/TiO <sub>2</sub> -3	0.015	0.485	3.0
PDVL/TiO <sub>2</sub> -4	0.020	0.480	4.0
PDVL/TiO <sub>2</sub> -5	0.025	0.475	5.0

### 2.4. Characterization

A comparison of the pure PDVL and TiO<sub>2</sub> nanoparticles crystalline structures with that of the PDVL/TiO<sub>2</sub> nanocomposites was carried out using XRD analysis on an X-ray diffractometer (RigakuDmax 2000, Rigaku, The Woodlands, TX, USA). The crystalline structures of all specimens were examined using a Cu anode tube, tube voltage of 40 KV/40 mA, and generator current of 100 mA. All samples were scanned in the 5–60° 2theta range at a scanning rate of 1.0 °C·min<sup>-1</sup>. The FTIR spectra of PDVL/TiO<sub>2</sub> hybrid materials and their pure components were recorded at 25 °C using a Perkin Elmer 1000 spectrophotometer (PerkinElmer, Waltham, MA, USA). In all cases, at least

32 scans with an accuracy of  $2 \text{ cm}^{-1}$  were signal-averaged. The film samples used in this analysis were transparent and sufficiently thin to satisfy the Beer-Lambert law. The surface morphologies of the polymer and nanocomposites were examined on a JEOL JSM 6360 (JEOL, Tokyo, Japan) scanning electronic microscope (SEM) with acceleration voltage of 20.00 kV. In order to reduce any build up deposited on the film surfaces, specimens were carefully coated with a thin layer of gold using a JEOL JFC-1600 Auto Fine Coater operated at 20 mA for 80 s prior to the analysis. The DSC thermograms of PDVL/TiO<sub>2</sub> nanocomposites and their components were performed on a Shimadzu DSC 60A (Shimadzu, Kyoto, Japan), previously calibrated with indium. All samples weighing between 11 and 15 mg were packed in aluminum pans before placing them in the DSC cell. The samples were scanned from  $-100^\circ\text{C}$  to  $+250^\circ\text{C}$  under an atmosphere of nitrogen gas at a heating rate of  $20^\circ\text{C}\cdot\text{min}^{-1}$ , and then maintained at  $200^\circ\text{C}$  for approximately 5 min to destroy nuclei that might act as crystal seeds. The samples were then cooled down from  $200^\circ\text{C}$  to  $20^\circ\text{C}$  at a constant rate of 5, 10, 15, and  $20^\circ\text{C}\cdot\text{min}^{-1}$ , separately. All the data were collected from the second scan run and none of the obtained thermograms revealed any traces of degradation. The glass transition temperature  $T_g$  was derived accurately from the thermograms as the midpoint in the variation of the heat capacity with temperature. The melting point  $T_m$  and crystallization temperature  $T_c$  were taken exactly at the summits of their peaks. The TGA thermograms of the pure PDVL and PDVL/TiO<sub>2</sub> nanocomposites were recorded on a TGA/DSC1 Mettler-Toledo thermogravimeter (Mettler-Toledo International Inc., Columbus, OH, USA) under nitrogen gas. Samples weighing between 10.0 and 12.0 mg were scanned between 25 and  $600^\circ\text{C}$  at a heating rate of  $20^\circ\text{C}\cdot\text{min}^{-1}$ .

### 3. Results and Discussion

#### 3.1. XRD Analysis

The XRD patterns of TiO<sub>2</sub> nanoparticles, pure PDVL, and their composites containing 1, 2, 3, 4, and 5 wt % of TiO<sub>2</sub> are shown in Figure 1. The pattern of the pure anatase phase of TiO<sub>2</sub> nanoparticles reveals the main diffraction peaks at  $2\theta$  localized at  $25.30$ ,  $37.80$ ,  $48.10$ ,  $53.90$ ,  $55.00$ ,  $62.80$ , and  $70.00^\circ$ , with those of the rutile phase at  $27.4$ ,  $36.1$ ,  $41.3$ , and  $56.6^\circ$ , which agrees with the standard spectrum (JCPDS No.: 88-1175 and 84-1286) [41]. The crystal size of TiO<sub>2</sub> particles was evaluated from the Scherrer equation [42,43]:

$$D = \frac{K \times \lambda}{\beta \cos\theta} \quad (1)$$

where the X-ray wavelength  $\lambda$  of Cu K $\alpha$  radiation is  $1.54 \text{ \AA}$ , the shape factor  $K$  is assigned a value of 0.90,  $\theta$  is the Bragg angle, and  $\beta$  is the half-height of angle diffraction. The reflecting peak at  $25.3^\circ$ , which is the (101) characteristic peak of TiO<sub>2</sub> anatase, is taken to determine the diameter of an average crystal, and  $\beta$  is 0.411. Both of the  $\beta$  values are converted to radians, and using the Scherrer formula, the calculated average sizes of the crystallite TiO<sub>2</sub> nanoparticles are estimated to be approximately 20 nm. The semi-crystalline structure of pure PDVL is closely related to its chain architecture. The XRD pattern of this polymer has two crystallographic reflections, which are probably indexed to the crystal PDVL structure. The sharp crystalline peaks localized at  $2\theta$   $22^\circ$  and  $24^\circ$  were assigned to diffraction of the (110) and (200) lattice planes, respectively [44], indicating that the PDVL probably crystallized in the ordinary crystal geometric structure. The crystallographic analysis conducted by Furuhashi indicated that PDVL crystallized with an orthorhombic unit cell structure [45]. The XRD patterns of the PDVL/TiO<sub>2</sub> nanocomposites show only the combined crystallographic reflections of their pure components, indicating the non-formation of new crystalline structures and proving the stability of the crystallinity of the TiO<sub>2</sub> nanoparticles in the composite. However, an important depression in the crystallinity of PDVL is observed when the amount of TiO<sub>2</sub> nanoparticles incorporated in the composite is increased.

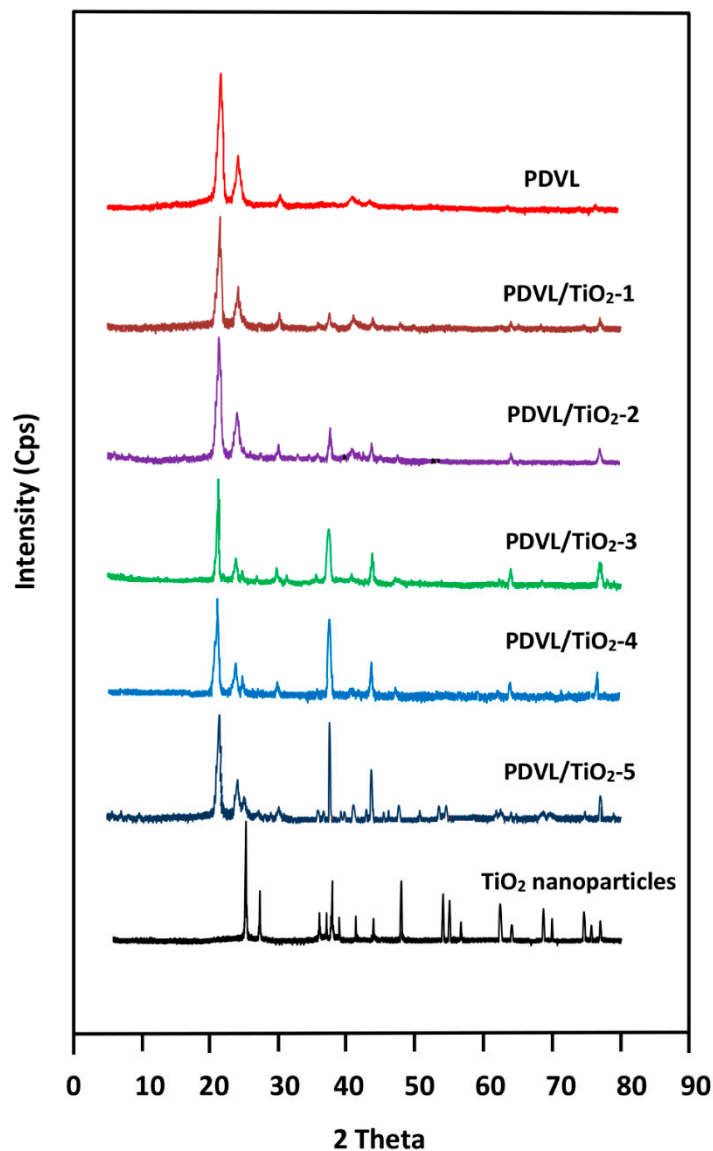


**Figure 1.** XRD refractograms of TiO<sub>2</sub> nanoparticles, pure PDVL, and their nanocomposites containing different TiO<sub>2</sub> contents.

### 3.2. SEM Analysis

The characteristics of multiphase systems such as nanocomposites are related to the nature and composition of the constituents, and also depend on the way they are prepared. The SEM micrographs of the purchased TiO<sub>2</sub> nanoparticles, pure PDVL, and PDVL/TiO<sub>2</sub> hybrid materials prepared by the solvent casting method, are shown in Figure 2. The photomicrograph in the middle shows typical nanosized TiO<sub>2</sub> before its dispersion in the PDVL matrix. The primary particles are sized between 17 and 26 nm in diameter. The micrograph in the top right shows the surface morphology of the pure PDVL film containing grafts or borrowings probably produced during the preparation of the film. On the other hand, those of the nanocomposites have grainy morphology surfaces whose nanoparticles are denser in the case of PDVL/TiO<sub>2</sub>-5, and appear well covered with PDVL and uniformly dispersed in the polymeric matrix in its nanoscale. As can be seen from these images, the particle-polymer adhesion seems to be quite rich, as revealed by the absence of voids around the TiO<sub>2</sub> filler. This finding confirms the good compatibility between TiO<sub>2</sub> and the PDVL polymer matrix revealed by the DSC analysis.

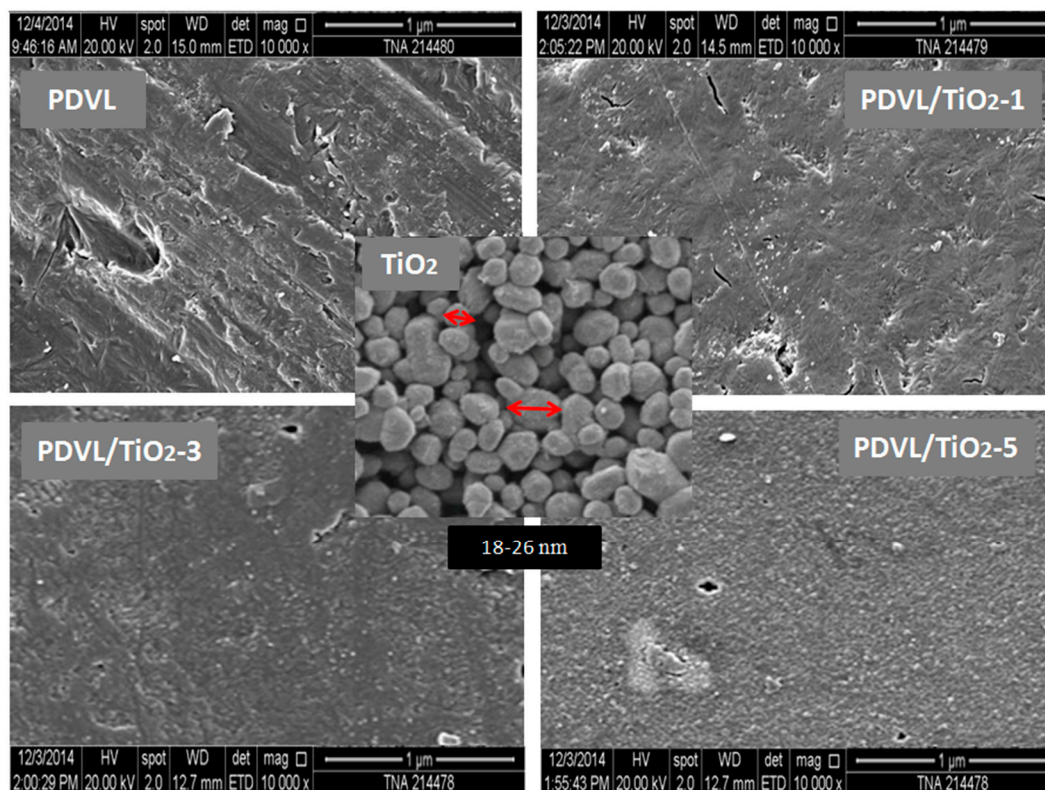


**Figure 2.** SEM micrographs of the surface morphologies of pure PDVL and PDVL/TiO<sub>2</sub> nanocomposites containing 1, 3, and 5 wt % TiO<sub>2</sub> contents.

### 3.3. FTIR Analysis

Figure 3 presents a comparison between the FTIR spectra of PDVL/TiO<sub>2</sub> nanocomposites and those of their components, and reveals no particular shift on the absorption bands of PDVL. However, a slight widening of the carbonyl band at 1730 cm<sup>-1</sup> at the half of its height is observed, indicating the presence of an interaction between the polymer and the nanofiller. This observation is also confirmed by the decrease in the broad band localized between 550 and 650 cm<sup>-1</sup> attributed to the Ti–O–Ti of TiO<sub>2</sub> in the hybrid materials. According to the literature [46,47], a depression in the carbonyl peaks of PCL in PCL/TiO<sub>2</sub> nanocomposites, in which PDVL is one of its family, is caused by the presence of an interaction between PCL chains and TiO<sub>2</sub> nanoparticles. Basing on this principle, we can confirm the presence of TiO<sub>2</sub> in the PDVL matrix in nanocomposite form.

### 3.4. Thermal Behavior of the PDVL/TiO<sub>2</sub> Nanocomposite

A uniform thermal history across all specimens was ensured by presenting thermograms with traces of the second run after quenching from temperatures slightly above  $T_g$ . As shown in Figure 4, the thermogram of PDVL shows that  $T_g$  and  $T_m$  occur at  $-63\text{ }^\circ\text{C}$  and  $58\text{ }^\circ\text{C}$ , respectively, which is in agreement with the literature [48,49]. The thermal curves of PDVL/TiO<sub>2</sub> systems show a dependence of the thermal properties on the TiO<sub>2</sub> content incorporated in the composite. Table 2 summarizes the  $T_g$ s and  $T_m$ s values deduced. As indicated by this table, the glass transition behavior is significantly influenced by the TiO<sub>2</sub> content, in which the  $T_g$  value of the PDVL in the PDVL/TiO<sub>2</sub> system increased from  $-63$  to  $-47\text{ }^\circ\text{C}$  when the TiO<sub>2</sub> loading was varied from 0 to 5 wt %. However, as the inorganic content increased, the melting behavior stabilized or slightly decreased, and the  $T_m$  value stabilized at approximately  $59\text{ }^\circ\text{C}$  or increased from  $58\text{ }^\circ\text{C}$  to  $60\text{ }^\circ\text{C}$ . The value of  $\Delta H_m$  decreased from 63 to  $52.5\text{ J}\cdot\text{g}^{-1}$ . This finding can be explained by a thermodynamic mixture accompanied by exothermic interactions created between the crystalline structure of PDVL and those of TiO<sub>2</sub> nanoparticles, in which the slide chains are considerably reduced, leading to an increase in  $T_g$  and a decrease in the enthalpy of melting.

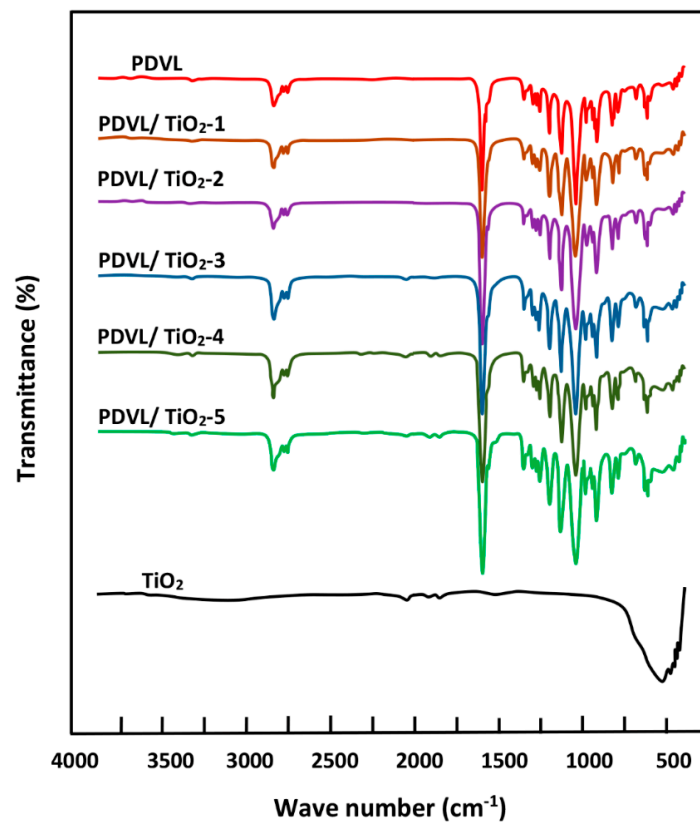


**Figure 3.** FTIR spectra of TiO<sub>2</sub> nanoparticles, pure PDVL, and PDVL/TiO<sub>2</sub> nanocomposites with different TiO<sub>2</sub> loadings.

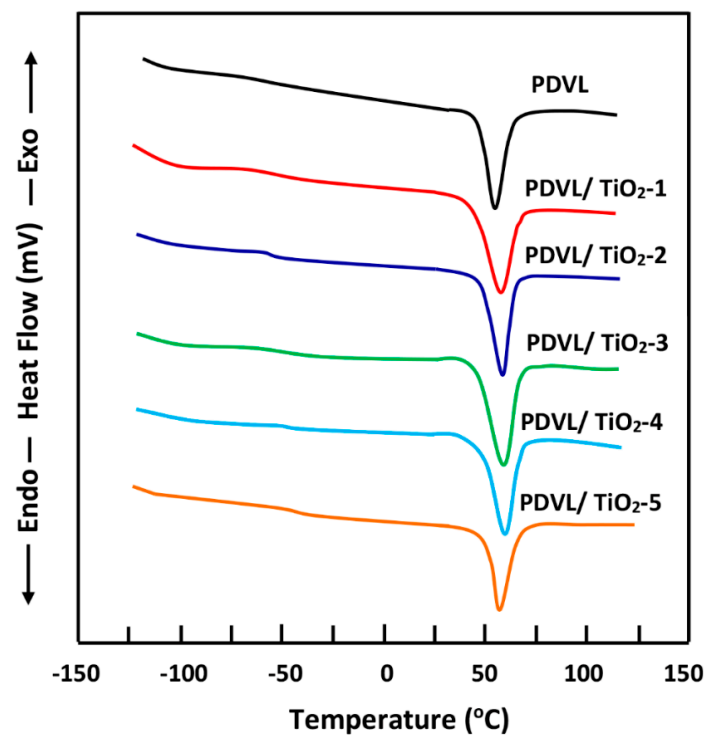


**Figure 4.** Differential scanning calorimetry (DSC) thermal curves of pure PDVL and PDVL/TiO<sub>2</sub> nanocomposites containing different TiO<sub>2</sub> contents taken in the heating mode with a heating rate of 20 °C·min<sup>-1</sup>.

**Table 2.** Glass transition temperatures and melting points of pure PDVL and PDVL/TiO<sub>2</sub> composites obtained at a heating rate of 20 °C·min<sup>-1</sup>.

System	T <sub>g</sub> (°C)	T <sub>m</sub> (°C)	ΔH <sub>m</sub> (J·g <sup>-1</sup> )	T <sub>c</sub> (°C)	ΔH <sub>c</sub> (J·g <sup>-1</sup> )	X <sub>c</sub> (%)
PDVL	-63	58	63.0	26	54.3	46.3
PDVL/TiO <sub>2</sub> -1	-60	58	59.7	28	52.2	40.0
PDVL/TiO <sub>2</sub> -2	-57	58	57.4	29	51.0	34.7
PDVL/TiO <sub>2</sub> -3	-54	59	56.0	30	50.0	33.0
PDVL/TiO <sub>2</sub> -4	-49	60	53.8	31	48.2	30.0
PDVL/TiO <sub>2</sub> -5	-47	56	52.5	32	47.3	29.0

As is well-known for polymer composites, the crystallization temperature of the polymer component depends on its affinity with respect to the filler, the physico-chemical properties of the two components, and crystallization conditions [50]. The DSC thermograms of pure PDVL and PDVL/TiO<sub>2</sub> nanocomposites recorded in the cooling mode are shown in Figure 5, and the temperatures and the heats of crystallization that were deduced are gathered in Table 2. The DSC thermogram of pure PDVL exhibits a crystallization temperature at 27 °C, which is slightly lower than that in the literature (29.7–30.4 °C) [44]. However, no significant change in the T<sub>c</sub> value of PDVL is observed when the amount of TiO<sub>2</sub> varied from 1 to 5 wt % is incorporated in the polymer matrix. On the other hand, a relatively dramatic depression of the crystallization heat (from 54.3 to 47.3 J·g<sup>-1</sup>) is observed for the same variation of the TiO<sub>2</sub> content.

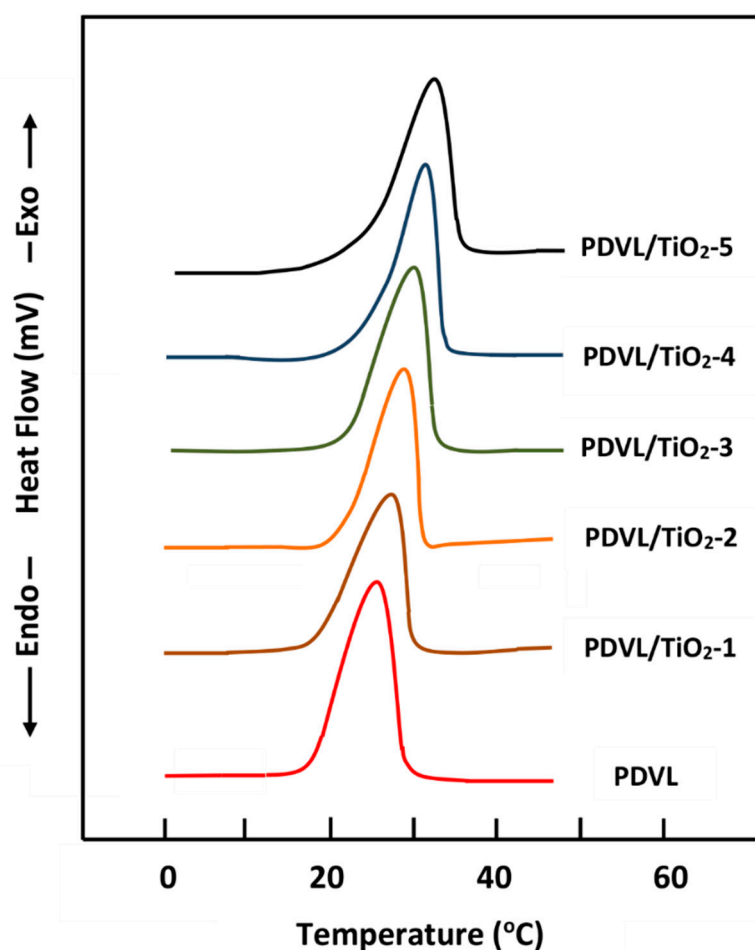
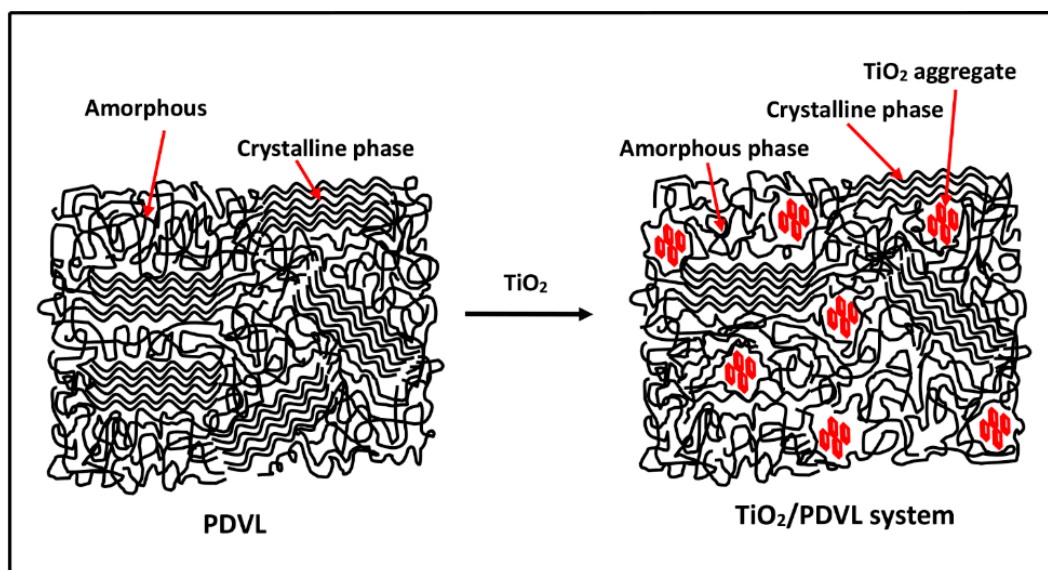


**Figure 5.** DSC thermograms of pure PDVL and PDVL/TiO<sub>2</sub> hybrid materials containing different TiO<sub>2</sub> contents taken in the cooling mode with a cooling rate of 20 °C·min<sup>-1</sup>.

The degree of crystallinity  $X_c$  of pure PDVL and PDVL/TiO<sub>2</sub> systems with different TiO<sub>2</sub> contents was determined using Equation (2) [44,51–53]:

$$X_c = \frac{\Delta H_m - \Delta H_c}{w_f \Delta H_m^0} \times 100 \quad (2)$$

where  $\Delta H_m$  is the heat attributed to fusion of PDVL;  $\Delta H_m^0$  is the enthalpy of fusion of 100% crystalline PDVL, which is estimated at 18.8 J·g<sup>-1</sup> [54]; and  $w_f$  is the weight fraction of PDVL in the composite. The degree of crystallinity of pure PDVL and those of PDVL/TiO<sub>2</sub> nanocomposites obtained by this method are shown in the data in Table 2. A significant decrease in  $X_c$  is observed with increasing TiO<sub>2</sub> content, revealing that the crystallinity rate of PDVL is significantly affected by this inorganic filler, notably at 5 wt % in the composite, in which this polymer loses approximately 13% of its crystallinity. This decrease in the crystallinity of PDVL in the nanocomposite is certainly due to the TiO<sub>2</sub> nanoparticles being incrustated between the polymer chains, which hinders the crystallization process and the formation of crystallites (Scheme 1). Comparable results were also obtained by Jiang et al. [55] using the PCL/SiO<sub>2</sub> nanomaterial. On the other hand, the thermograms of the pure PDVL and nanocomposites, realized at cooling rates ranging between 5 and 20 °C·min<sup>-1</sup> (shown in Figure 6), revealed that for all samples, the peak of the crystallization enthalpy shifted toward lower temperatures when the cooling rate increased. The high cooling rate prevents the motion of the macromolecular chains from following the cooling process in time, due to the influence of heat hysteresis, and this fact leads to a lower peak of the crystallization temperature. Therefore, the crystallization process is facilitated by the lower cooling rate.



**Scheme 1.** Suggested semi-crystalline structures of pure PDVL and the PDVL/TiO<sub>2</sub> nanocomposite.

The variation in the  $T_c$  value vs. the PDVL/TiO<sub>2</sub> composition at different cooling rates, plotted in Figure 7, revealed comparable profiles which increased linearly with the TiO<sub>2</sub> content. This finding indicates that the incorporation of TiO<sub>2</sub> nanoparticles in the PDVL matrix, ranging between 1.0 and 5.0 wt %, accelerates the crystallization process. Comparable results were also observed by Wang et al. [56] using the PCL/TiO<sub>2</sub> nanocomposite, and this phenomenon was attributed to an effect of heterogeneity nucleation of the nanoparticles in the polymer matrix.

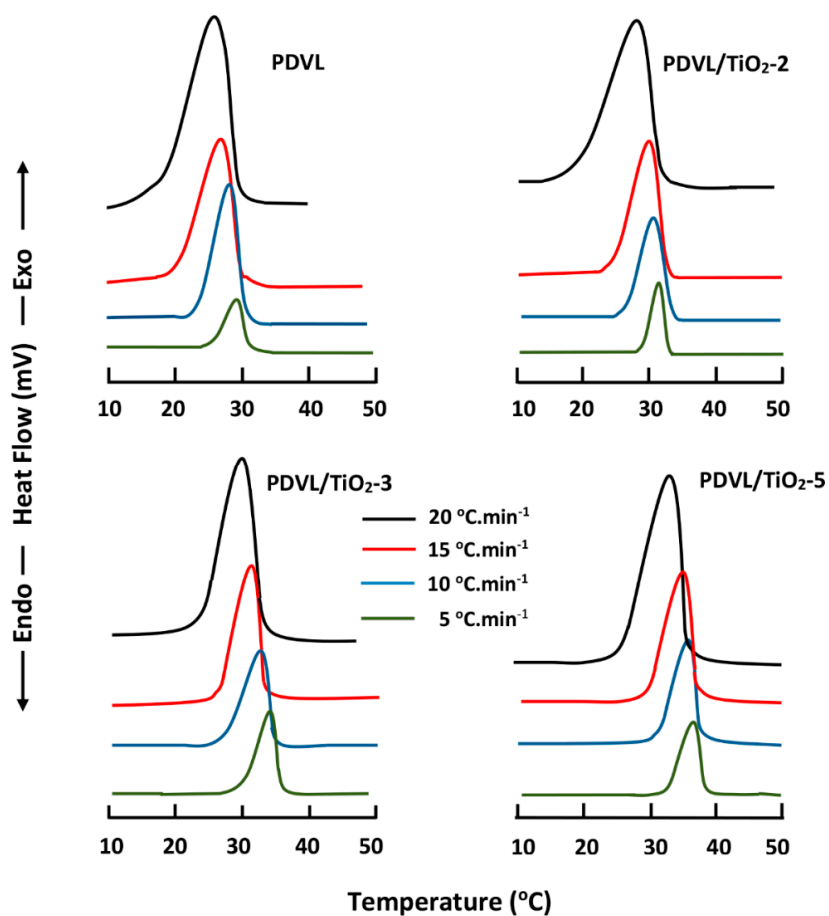


**Figure 6.** DSC thermal curves of pure PDVL and PDVL/TiO<sub>2</sub> hybrid systems with different TiO<sub>2</sub> contents obtained with different cooling rates.

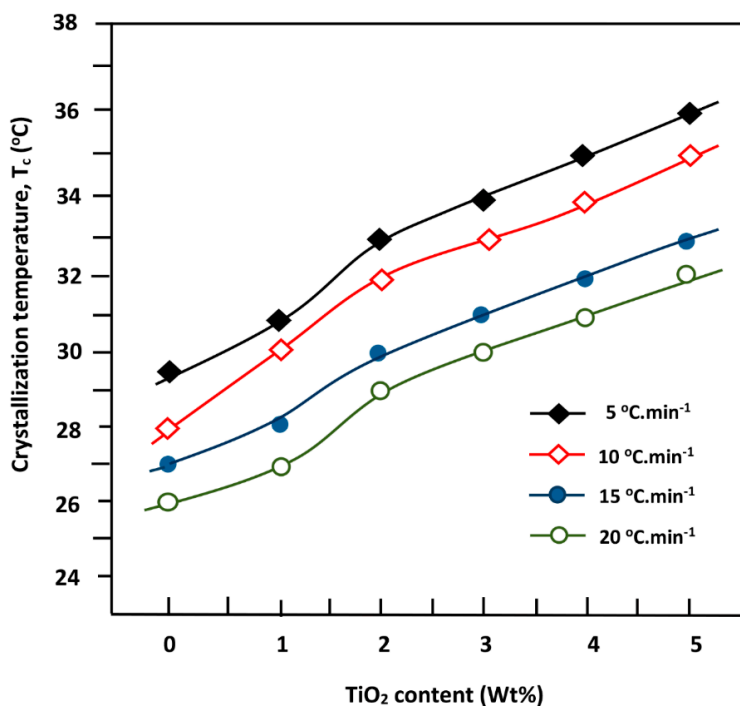


**Figure 7.** Variation of the maximum crystallization temperature  $T_c$  of pure PDVL and PDVL/TiO<sub>2</sub> nanocomposites versus composition.

### 3.5. Non-Isothermal Crystallization Kinetics of PDVL and PDVL/TiO<sub>2</sub> Nanocomposites

The relative degree of crystallinity  $X_T$  vs. the crystallization temperature is expressed by Equation (3) [57]:

$$X_T = \frac{A_T}{A_\infty} \quad (3)$$

$$\text{with } A_T = \int_{T_0}^T \left( \frac{dH}{dt} \right) dt \text{ and } A_\infty = \int_{T_0}^{T_\infty} \left( \frac{dH}{dt} \right) dt$$

where  $A_T$  is the area under the thermograms from  $T = T_0$  to  $T = T$ , and  $A_\infty$  is the total area under the crystallization curve. Further,  $T_0$  and  $T_\infty$  are the beginning and end of crystallization temperatures taken at the starting and finishing inflections of the crystallization peak, respectively, and  $H$  is the heat of the process. Based on Equation (3),  $X_T$  at a specific temperature  $T$  is calculated. During non-isothermal crystallization, the variation of the crystallization time with the crystallization temperature is given by Equation (4):

$$t = \frac{(T_0 - T)}{\beta} \quad (4)$$

where  $T$  is the temperature of crystallization at time  $t$ , and  $\beta$  is the cooling rate in degrees Celsius per minute. The integration of the exothermic peaks during the non-isothermal crystallization process leads to the attainment of the relative degree of crystallinity  $X_T$  as a function of temperature.

Figure 8 (on the left) shows the curves obtained for pure PDVL and the PDVL/TiO<sub>2</sub> nanocomposite containing 3 wt % of TiO<sub>2</sub> as an example. Because crystallization is impeded, all curves have a pattern approximating a sigmoid shape. A typical plot of  $X_t$  vs. time for pure PDVL, and this same system plotted using a combination of Equations (3) and (4), are also shown in Figure 8 (on the right). As in the case of the plots of  $X_T$  vs. temperature, all patterns have an approximately sigmoid profile, and their slopes at each point indicate the instantaneous rate of crystallization. As can be seen, the rate of crystallization is almost constant between 20% and 80% of the relative crystallinity, because the profile of these curves in this zone is almost a straight line. At a later stage, the curves tend to become flat due to spherulite impingement [58].

Among the many models that have been developed to study the kinetics of isothermal crystallization, there are very few that are suitable for non-isothermal kinetics, such as those proposed by Jeziorny [57], Ziabicki [58], and Ozawa [59]. In the present investigation, the Ozawa equation, which is written as

$$1 - X_T = \exp\left(-\frac{k_T}{\beta^m}\right) \quad (5)$$

is adopted to investigate the non-isothermal crystallization of the virgin PDVL and PDVL/TiO<sub>2</sub> hybrid nanomaterials, using 5, 10, 15, and 20 °C·min<sup>-1</sup> cooling rates, in which this relationship is an extension of the Avrami equation [60]:

$$1 - X_t = \exp(-kt^n) \quad (6)$$

This equation was originally used for the conversion of isothermal crystallization to non-isothermal crystallization, by assuming that the sample is cooled at a constant cooling rate. The term  $X_t$  represents the relative degree of crystallinity as a function of the crystallization time  $t$ .  $k$  and  $k_T$  are the constants of the crystallization kinetics rate and the cooling function of non-isothermal crystallization at a certain temperature  $T$ , respectively. Further,  $n$  and  $m$  are the isothermal Avrami and the non-isothermal Ozawa exponents, respectively, and depend on the size of the crystal growth.  $\beta$  is the cooling rate.

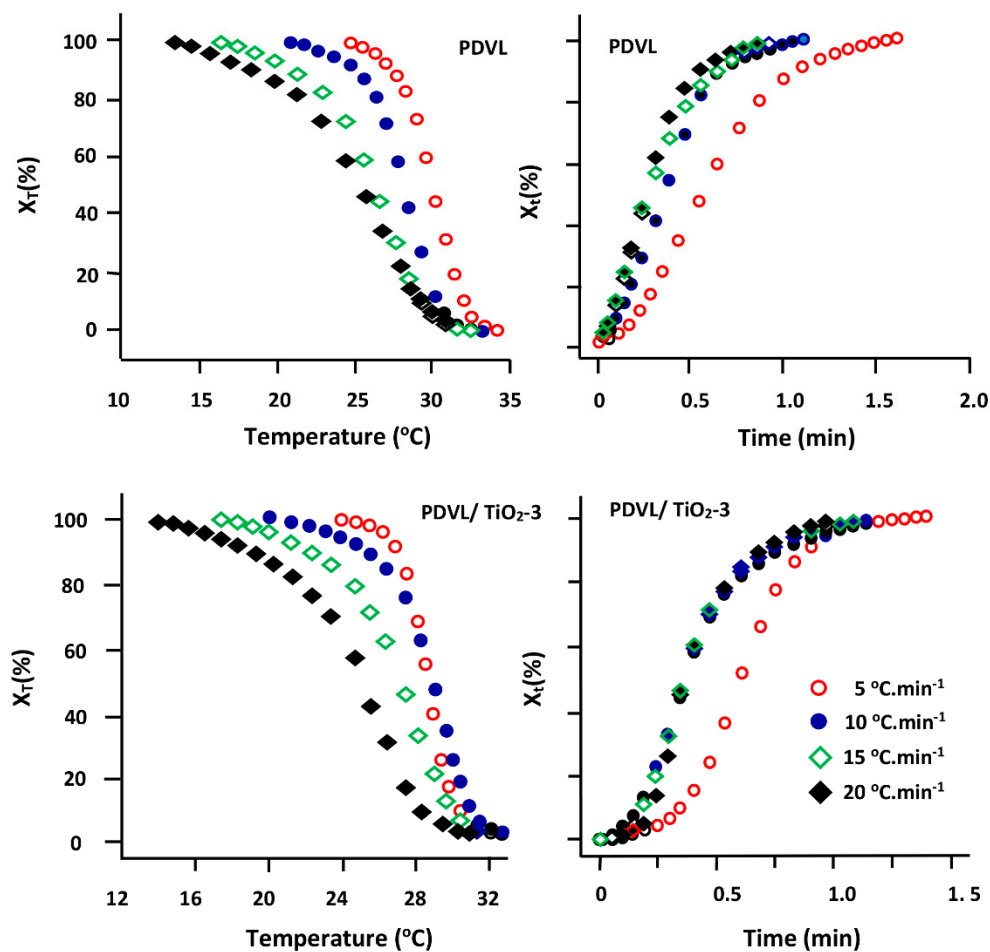


**Figure 8.** Sigmoid plots indicating the variation of the relative crystallization degree  $X_T$  and  $X_t$  for pure PDVL and the PDVL/TiO<sub>2</sub>-3 nanocomposite versus temperature and time, respectively.

When  $m$  or  $n$  is close to 3, this value indicates a crystalline growth in bulk or in three dimensions, whereas a value of  $m$  or  $n$  closer to 1 indicates surface growth. An intermediate  $n$  value between 1 and 3 indicates that both surface and internal crystallizations occur simultaneously [61]. Both parameters are determined from the linearized Equation (6) as follows:

$$\ln[-\ln(1 - X_T)] = \ln k_T - m \ln \beta \quad (7)$$

Plots of  $\ln[-\ln(1 - X_t)]$  vs.  $\ln(\beta)$  of virgin PDVL and the PDVL/TiO<sub>2</sub> systems containing different TiO<sub>2</sub> loadings are shown in Figure 9. A straight line is obtained, indicating that the Ozawa equation (Equation (7)) perfectly describes the main process of non-isothermal crystallization of pure PDVL and also that of the PDVL/TiO<sub>2</sub> system for all given compositions. The slope and the intercept of these curves yields the Ozawa exponent ( $m$ ) and crystallization kinetics rate ( $k_T$ ), respectively. The values of  $m$  and  $k_T$  of the pure polymer and composites are summarized in Table 3 and reveal that the average value of  $m$  for pure PDVL is close to 2. This finding indicates that the crystal evolves by growing in both dimensions, with a linear growth rate, a heterogeneous nucleation [62], and a thermal nucleation [63]. According to Desio et al. [64], a thermal nucleation implies that the nucleation rate does not contribute to the activation energy. However, the  $m$  values of the composites, which range from 1.60 to 3.10, slightly increase with the crystallization temperature, which is explained by the simultaneous appearance of two and three dimensional spherulitic growth. On the other hand, as for pure PDVL, the  $k_T$  value for each composite, of which the logarithm was between 3.38 and 7.32, increased with increasing the  $T_c$  value. These values indicate that the incorporation of a quantity of

TiO<sub>2</sub> nanoparticles ranging from 1.0% to 5.0% by weight in the PDVL matrix only slightly modifies the nucleation mechanism and the morphology of crystal growth.

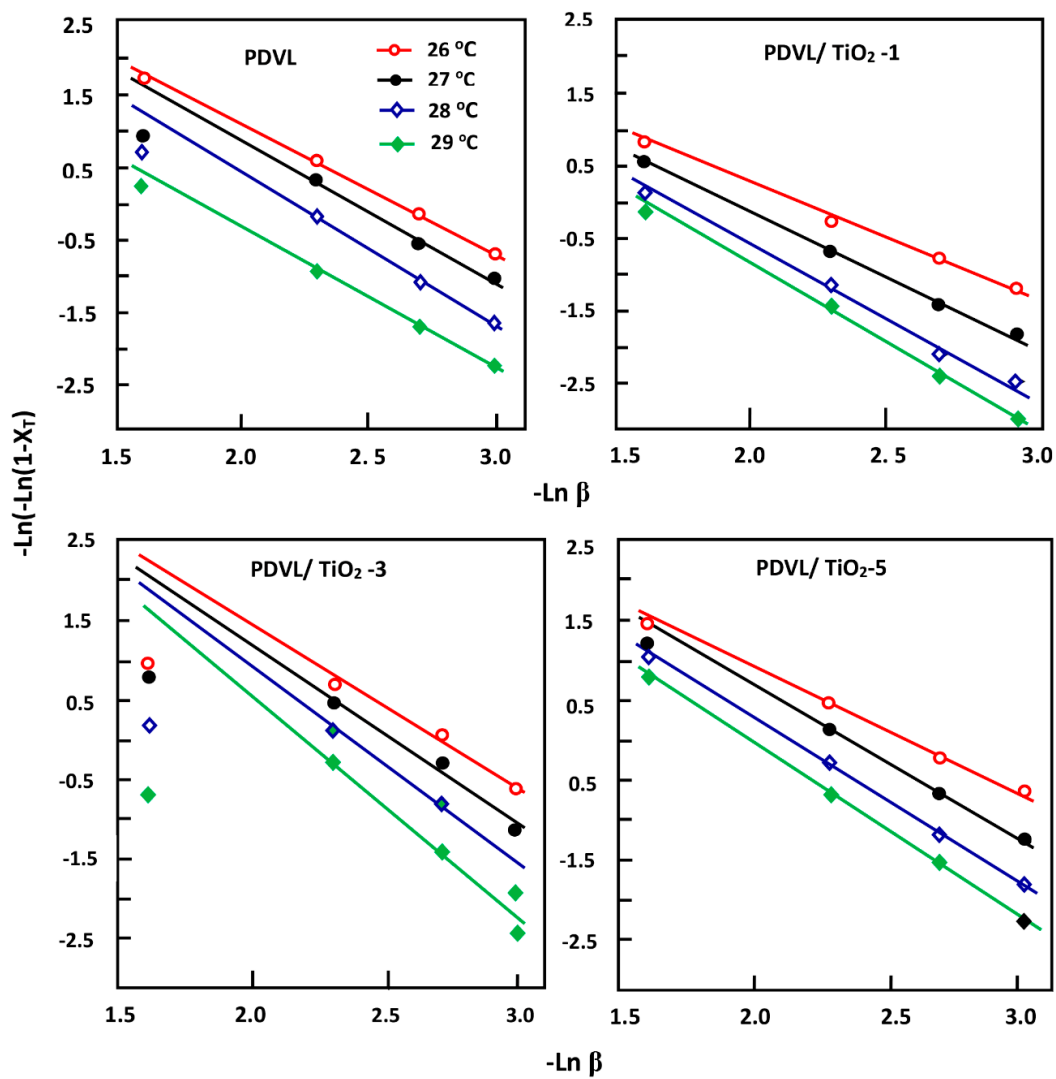


**Figure 9.** Ozawa plots indicating the variation of  $\ln[-\ln(1 - X_T)]$  vs.  $\ln \beta$  for pure PDVL and PDVL/TiO<sub>2</sub> systems containing 1, 3, and 5 wt % of TiO<sub>2</sub> loading.

**Table 3.** Ozawa parameters of virgin PDVL and PDVL/TiO<sub>2</sub> nanocomposites.

Sample	$T_c$ (°C)	$n$	$-\ln k_T$	$E_{ac}$ (kJ·mol <sup>-1</sup> )
PDVL	26	1.93	5.03	-214.10
	27	2.00	4.93	
	28	2.16	4.80	
	29	2.00	3.70	
PDVL/TiO <sub>2</sub> -1	26	1.60	3.48	-228.40
	27	2.00	4.15	
	28	2.12	3.67	
	29	2.20	3.56	
PDVL/TiO <sub>2</sub> -2	26	2.20	7.32	-266.05
	27	2.20	3.91	
	28	2.44	6.60	
	29	2.80	5.42	

Table 3. Cont.

Sample	$T_c$ (°C)	$n$	$-\ln k_T$	$E_{ac}$ (kJ·mol <sup>-1</sup> )
PDVL/TiO <sub>2</sub> -3	26	2.14	5.73	−377.13
	27	2.36	5.87	
	28	2.76	6.35	
	29	3.10	6.50	
PDVL/TiO <sub>2</sub> -4	26	1.70	4.37	−324.13
	27	1.94	4.56	
	28	1.96	4.18	
	29	2.02	4.08	
PDVL/TiO <sub>2</sub> -5	26	1.66	3.32	−277.13
	27	2.04	4.76	
	28	2.20	4.73	
	29	2.30	4.60	

The half time  $t_{1/2}$  toward complete crystallization of the pure PDVL and composites plotted in Figure 10A is deduced at 50% crystallinity of the curves of Figure 9, indicating the variation of  $X_t$  vs. time. These data reveal that the values of  $t_{1/2}$  were depressed following the same logarithmic profile when the cooling rate increased. A similar change in  $t_{1/2}$  was also observed by Wei et al. [65] using PCL/TiO<sub>2</sub> nanocomposites. Indeed, the  $t_{1/2}$  values obtained at 5 °C·min<sup>-1</sup> were approximately 2–5 times those at 20 °C·min<sup>-1</sup>, depending on the inorganic amount incorporated in the PDVL matrix. As can be seen, the  $t_{1/2}$  value of the sample containing 1 wt % TiO<sub>2</sub> dramatically decreased from 14.28 to 65.40 s when the cooling rate varied from 5 to 20 °C·min<sup>-1</sup>, whereas samples with TiO<sub>2</sub> content below 2 wt % decreased with a comparable trend. Figure 10B, in which  $t_{1/2}$  is presented vs. the TiO<sub>2</sub> content in the composite, reveals a lower dynamic of the crystallization process ( $t_{1/2}$  maximum) when 1 wt % of TiO<sub>2</sub> content was incorporated in the PDVL matrix, notably at the lowest cooling rate. In contrast,  $t_{1/2}$  reaches a minimum with 2 wt % of the filler in the composite, indicating a higher dynamic of the crystallization process, notably using the highest cooling rate. Another slowdown of the crystal growth, but less important, is also observed at 3–4 wt % of TiO<sub>2</sub> in the composite depending on the cooling rate used. This finding can be explained by the fact that at relatively low TiO<sub>2</sub> loadings, the filler cluster in the polymer matrix cannot restrict the motion of the PDVL macromolecular chains, but acts during the non-isothermal crystallization process as a heterogeneous nucleating agent and therefore increases the crystallization rate. However, at a higher TiO<sub>2</sub> loading, the titanium dioxide nanoparticles cluster to form a barrier that restricts the thermal motion of the PDVL macromolecules and therefore negatively impacts upon crystal formation. As a result, the incorporation of a large amount of TiO<sub>2</sub> in the PDVL matrix can delay the overall crystallization process.

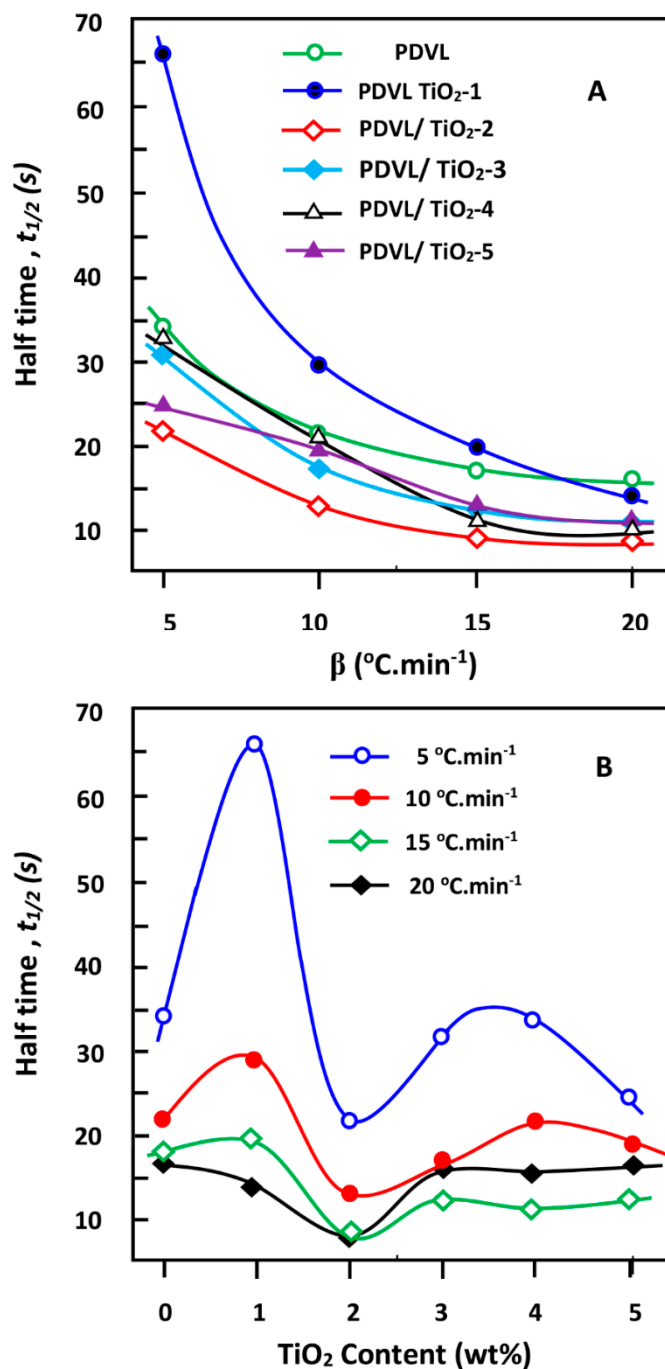


**Figure 10.** Variation of the  $t_{1/2}$  value of the crystallization of pure PDVL and PDVL/TiO<sub>2</sub> nanocomposites versus (A) the cooling rate and (B) TiO<sub>2</sub> content.

### 3.6. Activation Energy

The activation energy of crystallization  $E_{ac}$  is generally used to indicate the crystallization ability of polymers. Indeed, the lower the  $E_{ac}$  value, the higher the crystallization ability. In this work, the Kissinger equation [66] expressed below is used to estimate the  $E_{ac}$  values of pure PDVL and its composites:

$$E_{ac} = \frac{d[\ln(\beta/T_c^2)]}{d(1/T_c)} R \quad (8)$$

where  $R$  and  $T_c$  are the gas constant and the top of the crystallization temperature peak, respectively. The variation of  $\ln(\beta/T_c^2)$  vs.  $1/T_c$  for pure PDVL and its composites is plotted in Figure 11 and is

linear for all samples, and  $E_{ac}$  is deduced from the slope of each pattern with a correlation coefficient  $R^2$  exceeding 0.996. As shown in the data of Table 3, at any composition, the crystallization activation energy has negative values, indicating that the crystallization is an exothermic process. Furthermore,  $E_{ac}$  for the pure PDVL is  $-214.10 \text{ kJ}\cdot\text{mol}^{-1}$  and was surpassed by a maximum of  $-324.25 \text{ kJ}\cdot\text{mol}^{-1}$  when 4 wt % of  $\text{TiO}_2$  was added to the PDVL polymer matrix. According to Yang et al. [67], the more negative  $E_{ac}$  is, the more heat is released for crystallization and the more crystallization is favored. In other words, the incorporation of 4 wt % of  $\text{TiO}_2$  nanofiller in the PDVL polymer matrix greatly facilitated the crystallization of PDVL in the composite. This fact is gradually amortized with the addition of supplementary amounts of  $\text{TiO}_2$  in the nanocomposite. In general, the increase in the absolute value of  $E_{ac}$  should be due to the increase in the transportability of the PDVL chains, owing to the incorporation of  $\text{TiO}_2$  in the polymer matrix. The incorporation of  $\text{TiO}_2$  nanocomposite into the PDVL matrix could have heterogeneous nucleation effects; therefore, in this situation the hindrance effect of this load is not negligible. In the case of the incorporation of a small amount of  $\text{TiO}_2$  in the PDVL matrix, the heterogeneous effect is not obvious, while the chain mobility of the polymer decreases even more. In addition, the absolute values of  $E_{ac}$  of the PDVL/ $\text{TiO}_2$  nanocomposites are higher than that of pure PDVL. On the other hand, when the  $\text{TiO}_2$  content in the nanocomposite increased, its heterogeneous effect became even more important, despite the reduced mobility of the PDVL macromolecule chains.

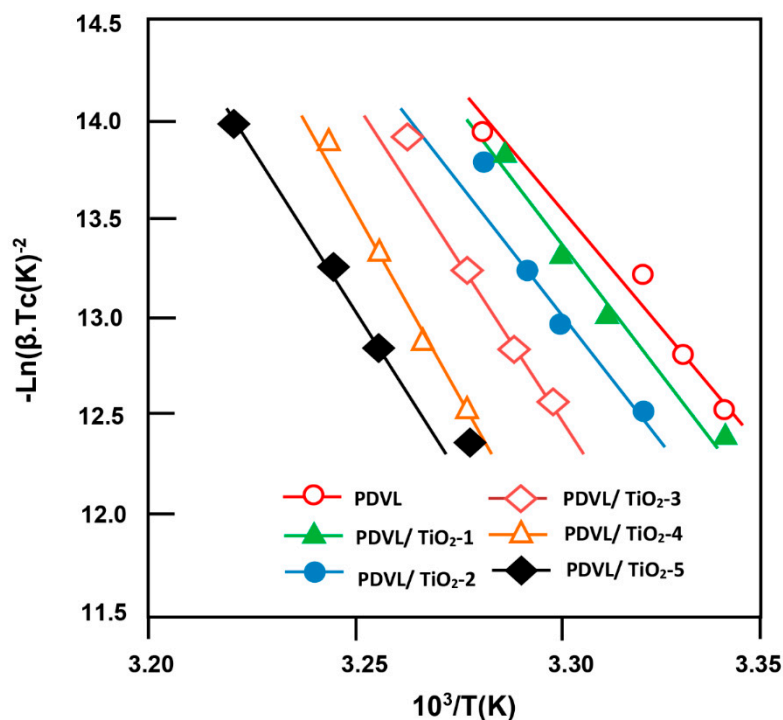


**Figure 11.** Kissinger plots indicating the variation of  $-\text{Ln}(\beta \cdot T_c^{-2})$  for pure PDVL and PDVL/ $\text{TiO}_2$  nanocomposites at different compositions versus the reverse of temperature.

### 3.7. Effective Energy Barrier

According to Vyazovkin [68], the Kissinger equation generally gives unspecified values of the activation crystallization energy, because the dependence of the temperature on the overall flow cannot be correctly described by a single Arrhenius graph on an extended temperature. On the other hand, the variation of the effective activation energy of the relative crystallinity ( $X_t$ ) has an additional parameter that is used to detect the change in the crystallization process that probably occurs in processes such as polymer crystallization. This dependence was very useful for the detection and elucidation of complicated dynamics in the polymeric materials. In this investigation, the Friedman

differential iso-conversional equation [69], as expressed below, was employed to evaluate the effective energy barrier  $E_X$ :

$$\ln\left(\frac{dX}{dt}\right)_{X,i} = k - \frac{E_X}{RT_{X,i}} \quad (9)$$

where  $\ln(dX/dt)$  represents the logarithm of the instantaneous crystallization rate of the polymer or composite as a function of time taken at a certain conversion  $X$ .  $T_{X,i}$  is the set of temperatures linked to the conversion  $X$  obtained at different selected cooling rates. The index  $i$  refers to a given individual cooling rate.

In the Friedman equation, the function of the instantaneous crystallization rate of the polymer ( $X_t$ ) is obtained from the integration of the measured crystallization rates, which is initially differentiated with regard to time to obtain  $dX/dt$ . In addition, from the selection of the appropriate degree of crystallinity, the  $dX/dt$  values at a certain conversion  $X$  are correlated to the corresponding crystallization temperature  $T_X$ , and  $E_x$  is deduced from the slope of the linear curve presented in Figure 12, indicating the variation of  $\ln(dX/dt)_{X_i}$  vs. the inverse of  $T_X$ . The variation in  $E_x$  of pure PDVL and the composites vs. the obtained  $X_t$  are plotted in Figure 13. As shown in these curve profiles, the effective energy barriers of pure PDVL and PDVL/TiO<sub>2</sub> nanocomposites have large negative values, and linearly increase with the extent of conversion and decrease in temperature. Comparable results were also observed by Wei et al. [65] using PCL as the polymer matrix, and this fact was attributed to the great difficulty of the polymer to crystallize as the crystallization progresses.

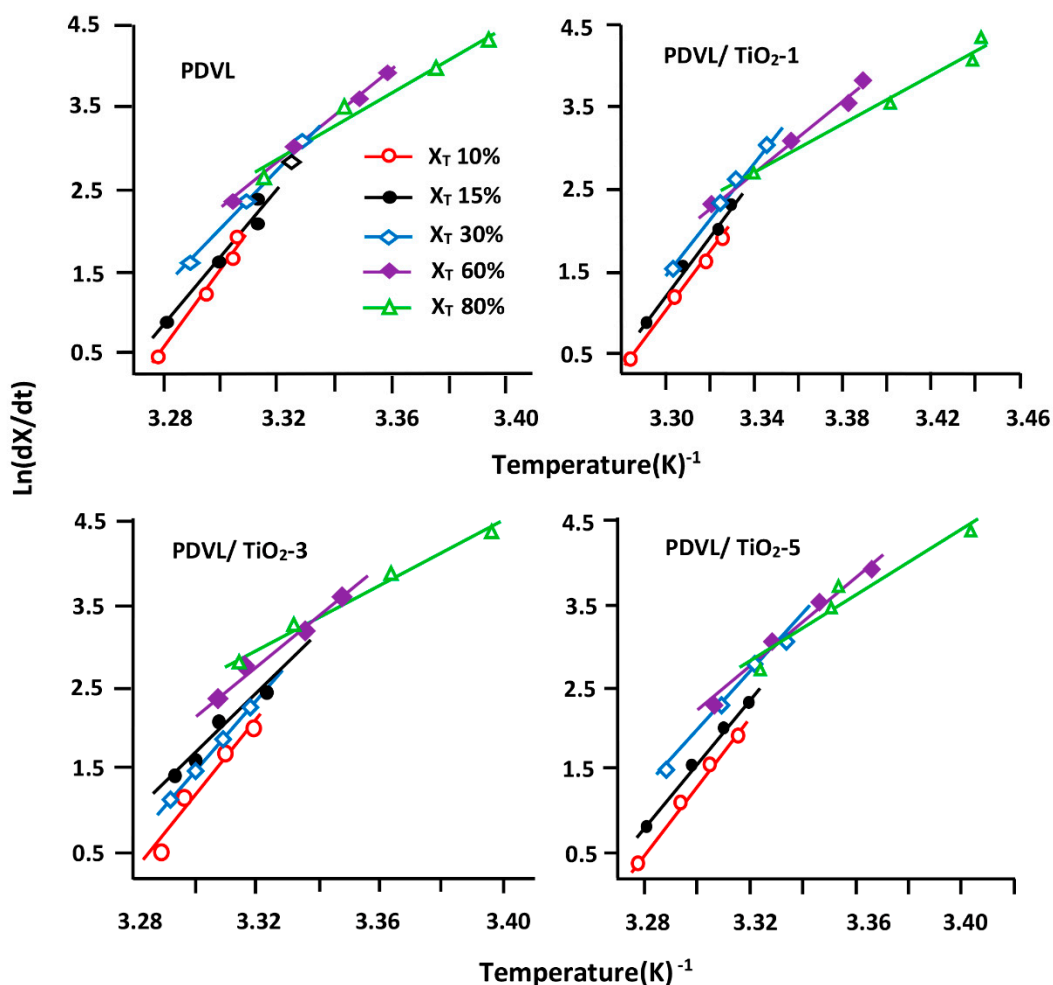


**Figure 12.** Variation of the instantaneous crystallization rate  $dX/dt$  versus the reverse of temperature for pure PDVL and PDVL/TiO<sub>2</sub> hybrid materials containing 1, 3, and 5 wt % of TiO<sub>2</sub> contents.

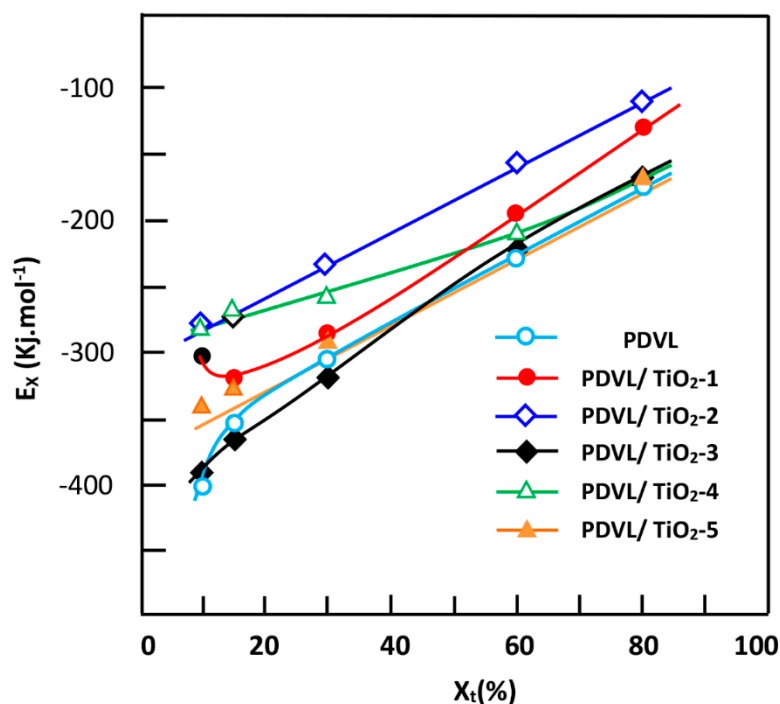


**Figure 13.** Curves indicating the variation of the effective energy barrier  $E_x$  vs. the relative crystallization  $X_t$  for the pure PDVL and PDVL/TiO<sub>2</sub> hybrid materials containing different TiO<sub>2</sub> contents.

In this case, during the crystallization process, the diffusion of the crystallization chain segments during the progression of the fusion to the growth front is prevented by the rejection of the segments of the polymer chain. Similar shapes were also obtained for polyethylene terephthalate (PET) and polypropylene/SiO<sub>2</sub> nanocomposites [70].

Considering the data in Figure 13, it is noteworthy that the nanocomposites exhibit higher values, indicating that the crystallization is hindered compared with that of PCL, except for the sample containing 3 wt % of TiO<sub>2</sub>, in which the crystallization process occurs at approximately the same or at slightly lower rates than the neat polymer. The tendency of the effective energy barrier evaluated using the iso-conversional method perfectly agrees with that obtained by the aforementioned Kissinger's route.

### 3.8. TGA Analysis

In contrast to poly ( $\delta$ -caprolactone) and poly(L-lactic acid), which are linear aliphatic polyesters, only a few investigations on the degradation behavior of PDVL have been reported [71,72]. In this work, the thermal degradation of pure PDVL and PDVL/TiO<sub>2</sub> nanocomposites was performed by the TGA method, and the thermograms obtained in nitrogen gas atmosphere are grouped in Figure 14. As shown in the thermal curve of pure PDVL, only one main decomposition step, which starts at 225 °C, is attributed to the formation of 4-pentanoic acid and carbon dioxide, similar to that observed during the thermal decomposition of the analogous PCL [73]. The curve profiles of the composites reveal an important shift of the onset of the decomposition of PDVL from 225 °C to 265 °C with increasing TiO<sub>2</sub> loading, thereby indicating a significant improvement in its thermal stability. The thermograms of the PDVL/TiO<sub>2</sub> systems also showed a second decomposition step, which started at 372 °C for the PDVL/TiO<sub>2</sub>-1 nanocomposite containing 1 wt % of TiO<sub>2</sub> nanoparticles, and dramatically shifted to 400 °C for that containing 5 wt % of TiO<sub>2</sub>. During this step, this material lost between 15 and 40 wt % of its weight, which was volatilized depending on the amount of nanofiller in the PDVL matrix. An unexpected observation in the form of a second decomposition step can be seen in the

PDVL/TiO<sub>2</sub> nanocomposite thermograms. This step started at 400–420 °C, and was completed at 420 and 475 °C depending on the amount of TiO<sub>2</sub> incorporated in the nanocomposite. During this step, the degradation of this hybrid material slowed down, and between 5 and 35 wt % of the material was degraded depending on its PDVL/TiO<sub>2</sub> composition. The presence of TiO<sub>2</sub> nanoparticles in this temperature range seems to interact with the residual sample to produce new molecules. This suggestion can also explain the increase in weight loss during this step, as the TiO<sub>2</sub> content in the nanocomposite increases.

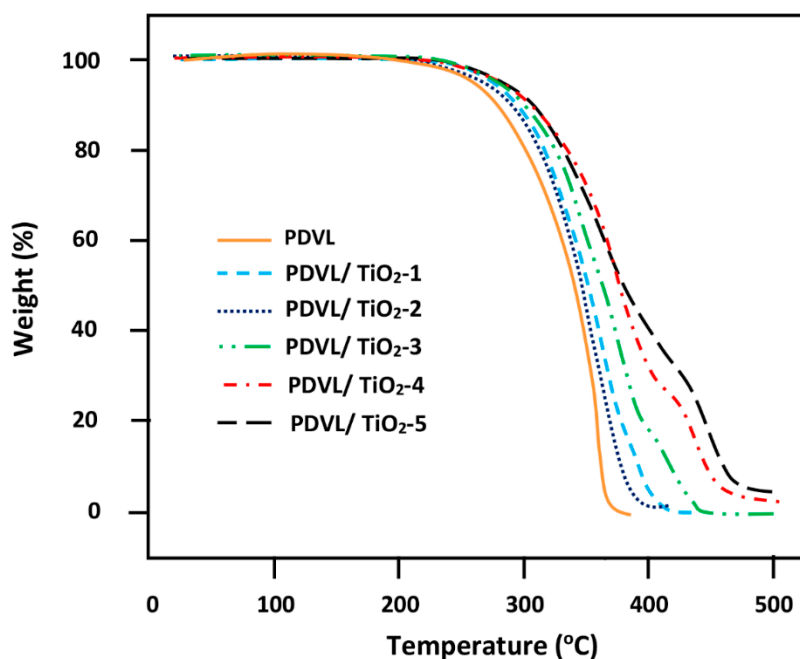


**Figure 14.** TGA thermograms of pure PDVL and PDVL/TiO<sub>2</sub> nanocomposites with different TiO<sub>2</sub> contents.

The activation energy  $E_a$  of the pure PDVL and PDVL/TiO<sub>2</sub> nanocomposites was estimated from the first stage of the thermal decomposition using the integral method proposed by Broido [74]:

$$\ln \left[ \ln \left( \frac{1}{Y} \right) \right] = -\frac{E_a}{RT} + C \quad (10)$$

$$\text{with } Y = \frac{w_T - w_\infty}{w_0 - w_\infty}$$

where  $Y$  represents the fraction of the sample not yet decomposed, and  $w_0$ ,  $w_\infty$ , and  $w_T$  are the initial weight, final weight, and the weight at a certain temperature, respectively. The variation of  $\ln \left[ \ln \left( \frac{1}{Y} \right) \right]$  versus the inverse of temperature plotted for pure PDVL and the nanocomposites in Figure 15 is linear, thus the  $E_a$  of the thermal decomposition process was deduced from the respective slopes. As can be seen from these curve profiles, the activation energy of pure PDVL was determined as 79.0 kJ·mol<sup>-1</sup>, which is lower than that reported in the literature (101 ± 10 kJ·mol<sup>-1</sup>) [73]. The activation energy increased to reach a maximum of 103.1 kJ·mol<sup>-1</sup> when the TiO<sub>2</sub> content in the nanocomposite is 2.0 wt %, beyond which it decreased to reach a minimum of 83.1 kJ·mol<sup>-1</sup> with the PDVL/TiO<sub>2</sub> system containing 5 wt % of TiO<sub>2</sub>. This finding indicates that the addition of a small amount of TiO<sub>2</sub> nanoparticles to this polymer enhanced the thermal stability of PDVL, notably when the percentage of TiO<sub>2</sub> in the composite is 2 wt %. The decrease in the  $E_a$  value when the nanofiller loading the composites increased is probably due to the lower energy required for bond scission and the unzipping of PDVL/TiO<sub>2</sub> nanocomposites.

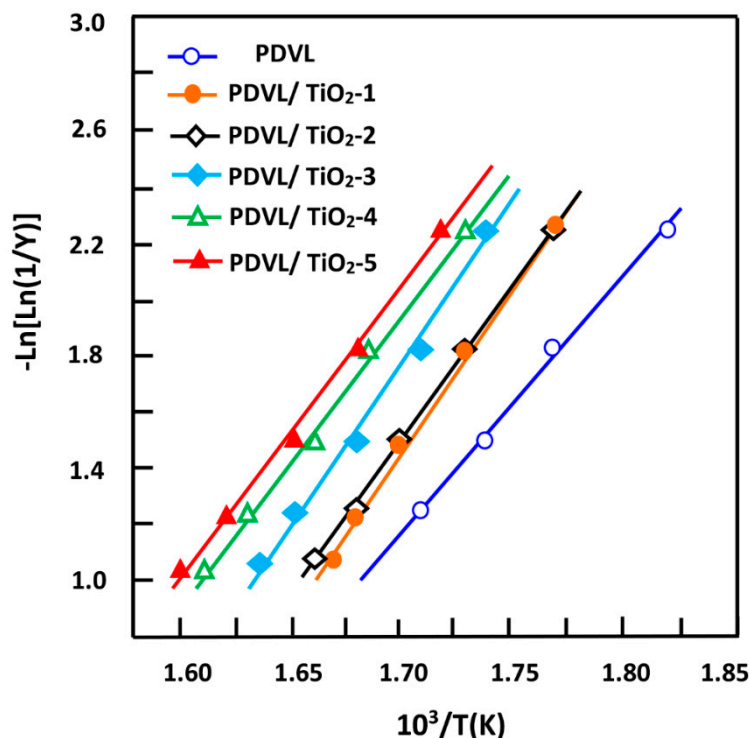


**Figure 15.** Variation of  $\text{Ln}[\text{Ln}(1/Y)]$  versus the reverse of temperature for pure PDVL and PDVL/TiO<sub>2</sub> nanocomposites containing different TiO<sub>2</sub> contents.

#### 4. Conclusions

In conclusion, the principal goal of this investigation is reached. Indeed, the preparation of a new nanocomposite material based on PDVL and TiO<sub>2</sub> nanoparticles by the solvent casting technique, with the aim of enhancing some of their properties, was attained. Indeed, the results obtained by DSC and XRD revealed that the TiO<sub>2</sub> nanoparticles are dispersed at the nanoscale in the polymer matrix. The XRD analysis of the PDVL/TiO<sub>2</sub> nanocomposites indicated the non-formation of new crystalline structures, thus proving the stability of the crystallinity of the TiO<sub>2</sub> nanoparticles in the composite. The DSC analysis revealed that the glass transition behavior is significantly affected by the addition of TiO<sub>2</sub> nanoparticles, and the crystallization rate of PDVL is significantly affected by the TiO<sub>2</sub> nanoparticles. The DSC analysis used at different cooling rates indicated that the incorporation of 1.0 to 5.0 wt % of TiO<sub>2</sub> nanoparticles in the PDVL matrix accelerates the crystallization process.

The non-isothermal crystallization kinetics of the PDVL/TiO<sub>2</sub> system revealed that the crystallization process involves a simultaneous occurrence of 2- and 3-dimensional spherulitic growth. The incorporation of between 1.0 and 5.0 wt % of TiO<sub>2</sub> nanoparticles in the PDVL matrix does not sensibly alter the dynamic of nucleation and the morphology of crystal growth. When relatively small amounts of TiO<sub>2</sub> are incorporated into the PDVL matrix, the half-time values revealed that the nonofiller cluster in the polymer matrix could not restrict the movement of the PDVL molecular chains, but acts as a heterogeneous nucleating agent during the non-isothermal crystallization process, and therefore accelerates this process.

The crystallization activation energy of PDVL/TiO<sub>2</sub> estimated by the Kissinger equation revealed that the incorporation of 1 wt % of TiO<sub>2</sub> content in the polymer greatly facilitated the crystallization of PDVL in the composite. This fact is gradually amortized with the addition of increasing amounts of TiO<sub>2</sub> in the nanocomposite. In general, the variation of the energy barrier  $E_x$  of pure PDVL and PDVL/TiO<sub>2</sub> nanocomposites vs.  $X_t$  shows a difficulty of crystallization for this polymer. During the crystallization process, the diffusion of the segments of the crystallization chain during the progression of the fusion at the growth front is prevented by the rejection of the segments of the polymer chain.

The thermal degradation analysis of PDVL/TiO<sub>2</sub> nanocomposites reveals a significant improvement in the thermal stability of PDVL. According to the degradation activation energy obtained by the Broido equation, the incorporation of a small TiO<sub>2</sub> amount enhanced the thermal stability of PDVL.

**Author Contributions:** Conceptualization, A.A.A.; Data curation, A.-B.A.-O.; Formal analysis, W.S.S.; Funding acquisition, A.A.A. and A.A.; Investigation, A.-B.A.-O.; Methodology, W.S.S.; Project administration, T.A.; Validation, A.A.; Writing—original draft, W.S.S. and T.A.; Writing—review & editing, T.A.

**Funding:** The authors are grateful to the Deanship of Scientific Research, King Saud University for funding through Vice Deanship of Scientific Research Chairs, Engineer Abdullah Bugshan research chair for Dental and Oral Rehabilitation.

**Conflicts of Interest:** The authors declare no conflict of interest. The funders had no role in the design of the study; in the collection, analysis, or interpretation of data; in the writing of the manuscript; or in the decision to publish the results.

## References

1. Coombes, A.; Rizzi, S.; Williamson, M.; Barralet, J.; Downes, S.; Wallace, W. Precipitation casting of polycaprolactone for applications in tissue engineering and drug delivery. *Biomaterials* **2004**, *25*, 315–325. [[CrossRef](#)]
2. Woodruff, M.A.; Hutmacher, D.W. The return of a forgotten polymer—Polycaprolactone in the 21st century. *Prog. Polym. Sci.* **2010**, *35*, 1217–1256. [[CrossRef](#)]
3. Khalil, M.I.A.-S.; Al-Deyab, S.S. Synthesis of poly ( $\delta$ -valerolactone) by activated monomer polymerization, its characterization and potential medical application. *Asian J. Biochem. Pharm. Res.* **2015**, *5*, 137–147.
4. Vaida, C.; Takwa, M.; Martinelle, M.; Hult, K.; Keul, H.; Möller, M.  *$\Gamma$ -Acyloxy- $\epsilon$ -Caprolactones: Synthesis, Ring-Opening Polymerization vs. Rearrangement by Means of Chemical and Enzymatic Catalysis*; Wiley Online Library: Hoboken, NJ, USA, 2008; pp. 28–38.
5. D’auria, I.; Mazzeo, M.; Pappalardo, D.; Lamberti, M.; Pellecchia, C. Ring-opening polymerization of cyclic esters promoted by phosphido-diphosphine pincer group 3 complexes. *J. Polym. Sci. Part A Polym. Chem.* **2011**, *49*, 403–413. [[CrossRef](#)]
6. Albertsson, A.-C.; Varma, I.K. Recent developments in ring opening polymerization of lactones for biomedical applications. *Biomacromolecules* **2003**, *4*, 1466–1486. [[CrossRef](#)] [[PubMed](#)]
7. Grobelny, Z.; Matlengiewicz, M.; Skrzeczyna, K.; Swinarew, A.; Golba, S.; Jurek-Suliga, J.; Michalak, M.; Swinarew, B. Ring-opening polymerization of lactones initiated with metal hydroxide-activated macrocyclic ligands: Determination of mechanism and structure of polymers. *Int. J. Polym. Anal. Charact.* **2015**, *20*, 457–468. [[CrossRef](#)]
8. Nair, L.; Jagadeeshan, S.; Nair, S.A.; Kumar, G.V. Evaluation of triblock copolymeric micelles of  $\delta$ -valerolactone and poly (ethylene glycol) as a competent vector for doxorubicin delivery against cancer. *J. Nanobiotechnol.* **2011**, *9*, 42. [[CrossRef](#)] [[PubMed](#)]
9. Kim, T.; Lee, M.; Lee, S.; Park, Y.; Jung, C.; Boo, J.-H. Development of surface coating technology of tio2 powder and improvement of photocatalytic activity by surface modification. *Thin Solid Films* **2005**, *475*, 171–177. [[CrossRef](#)]
10. Brady, G.S.; Clauser, H.R.; Vaccari, J.A. *Materials Handbook*; McGraw-Hill: New York, NY, USA, 1956.
11. Zhang, Q.; Gao, L.; Guo, J. Effect of hydrolysis conditions on morphology and crystallization of nanosized TiO<sub>2</sub> powder. *J. Eur. Ceram. Soc.* **2000**, *20*, 2153–2158. [[CrossRef](#)]
12. Sivakumar, S.; Pillai, P.K.; Mukundan, P.; Warriar, K.G.K. Sol-gel synthesis of nanosized anatase from titanyl sulfate. *Mater. Lett.* **2002**, *57*, 330–335. [[CrossRef](#)]
13. Devi, M.; Panigrahiand, M.R.; Singh, U.P. Synthesis of TiO<sub>2</sub> nanocrystalline powder prepared by sol-gel technique using TiO<sub>2</sub> powder reagent. *Adv. Appl. Sci. Res.* **2014**, *5*, 140–145.
14. Pusit, P.; Sukon, P. Titanium dioxide powder prepared by a sol-gel method. *J. Ceram. Process. Res.* **2009**, *10*, 167–170.
15. Santana-Aranda, M.A.; Morán-Pineda, M.; Hernández, J.; Castillo, S. Physical properties of TiO<sub>2</sub> prepared by sol-gel under different pH conditions for photocatalysis. *Superficies y Vacío* **2005**, *18*, 46–49.
16. Mishra, A.; Kumar, S.B.; Roy, D. Development of Nano-TiO<sub>2</sub> by Mechanical Milling. *Int. J. Sci. Eng. Res.* **2015**, *4*, 2347–3878.

17. Park, S.D.; Cho, Y.H.; Kim, W.W.; Kim, S.J. Understanding of Homogeneous Spontaneous Precipitation for Monodispersed TiO<sub>2</sub> Ultrafine Powders with Rutile Phase around Room Temperature. *Solid State Chem.* **1999**, *146*, 230–238. [[CrossRef](#)]
18. Yin, H.; Wada, Y.; Kitamura, T.; Kambe, S.; Murasawa, S.; Mori, H.; Sakata, T.; Yanagida, S. Hydrothermal synthesis of nanosized anatase and rutile TiO<sub>2</sub> using amorphous phase TiO<sub>2</sub>. *J. Mater. Chem.* **2001**, *11*, 1694–1703. [[CrossRef](#)]
19. McCormick, J.R.; Zhao, B.; Rykov, A.; Wang, H.; Chen, J.G. Thermal Stability of Flame-Synthesized Anatase TiO<sub>2</sub> Nanoparticles. *J. Phys. Chem. B* **2004**, *108*, 17398–17402. [[CrossRef](#)]
20. Docters, T.; Chovelon, J.M.; Herrmann, J.M.; Deloume, J.P. Syntheses of TiO<sub>2</sub> photocatalysts by the molten salts method: Application to the photocatalytic degradation of Prosulfuron<sup>®</sup>. *Appl. Catal. B Environ.* **2004**, *50*, 219–226. [[CrossRef](#)]
21. Avvakumov, E.; Senna, M.; Kosova, N. *Soft Mechanochemical Synthesis: A Basis for New Chemical Technologies*; Kluwer Academic Publishers: Dordrecht, The Netherlands, 2001; p. 2.
22. Billik, P.; Plesch, G. Mechanochemical synthesis of anatase and rutile nanopowders from TiOSO<sub>4</sub>. *Mater. Lett.* **2007**, *61*, 1183–1186. [[CrossRef](#)]
23. Li, B.; Wang, X.; Yan, M.; Li, L. Preparation and characterization of nano-TiO<sub>2</sub> powder. *Mater. Chem. Phys.* **2003**, *78*, 184–188. [[CrossRef](#)]
24. Cornelius, C.J.; Marand, E. Hybrid inorganic–organic materials based on a 6FDA–6FpDA–DABA polyimide and silica: Physical characterization studies. *Polymer* **2002**, *43*, 2385–2400. [[CrossRef](#)]
25. Kasseh, A.; Ait-Kadi, A.; Riedl, B.; Pierson, J. Organic/inorganic hybrid composites prepared by polymerization compounding and controlled free radical polymerization. *Polymer* **2003**, *44*, 1367–1375. [[CrossRef](#)]
26. West, J.; Hench, L. The sol-gel process. *Chem. Rev.* **1990**, *90*, 33–72.
27. Tien, Y.; Wei, K. High-tensile-property layered silicates/polyurethane nanocomposites by using reactive silicates as pseudo chain extenders. *Macromolecules* **2001**, *34*, 9045–9052. [[CrossRef](#)]
28. Gonzalez-Oliver, C.; James, P.F.; Rawson, H. Silica and silica-titania glasses prepared by the sol-gel process. *J. Non-Cryst. Solids* **1982**, *48*, 129–152. [[CrossRef](#)]
29. Wang, K.H.; Chung, I.J.; Jang, M.C.; Keum, J.K.; Song, H.H. Deformation behavior of polyethylene/silicate nanocomposites as studied by real-time wide-angle x-ray scattering. *Macromolecules* **2002**, *35*, 5529–5535. [[CrossRef](#)]
30. Mendoza-Serna, R.; Bosch, P.; Padilla, J.; Lara, V.; Méndez-Vivar, J. Homogeneous Si-Ti and Si-Ti-Zr polymeric systems obtained from monomeric precursors. *Non-Cryst. Solids* **1997**, *217*, 30–40. [[CrossRef](#)]
31. Ganguli, S.; Dean, D.; Jordan, K.; Price, G.; Vaia, R. Mechanical properties of intercalated cyanate ester-layered silicate nanocomposites. *Polymer* **2003**, *44*, 1315–1319. [[CrossRef](#)]
32. Que, W.; Sun, Z.; Zhou, Y.; Lam, Y.; Chan, Y.; Kam, C. Optical and mechanical properties of tio<sub>2</sub>/sio<sub>2</sub>/organically modified silane composite films prepared by sol-gel processing. *Thin Solid Films* **2000**, *359*, 177–183. [[CrossRef](#)]
33. Chiang, C.L.; Ma, C.C.M.; Wu, D.L.; Kuan, H.C. Preparation, characterization, and properties of novolac-type phenolic/sio<sub>2</sub> hybrid organic–inorganic nanocomposite materials by sol-gel method. *J. Polym. Sci. Part A Polym. Chem.* **2003**, *41*, 905–913. [[CrossRef](#)]
34. Méndez-Vivar, J.; Mendoza-Serna, R.; Bosch, P.; Lara, V. Influence of isoeugenol as a chelating agent on the structure of Si–Ti polymeric systems obtained from alkoxides. *J. Non-Cryst. Solids* **1999**, *248*, 147–158. [[CrossRef](#)]
35. Lu, S.; Melo, M.M.; Zhao, J.; Pearce, E.M.; Kwei, T. Organic-inorganic polymeric hybrids involving novel poly (hydroxymethylsiloxane). *Macromolecules* **1995**, *28*, 4908–4913. [[CrossRef](#)]
36. Yu, Y.-Y.; Chen, C.-Y.; Chen, W.-C. Synthesis and characterization of organic–inorganic hybrid thin films from poly (acrylic) and monodispersed colloidal silica. *Polymer* **2003**, *44*, 593–601. [[CrossRef](#)]
37. Oh, W.; Hwang, Y.; Park, Y.; Ree, M.; Chu, S.-H.; Char, K.; Lee, J.; Kim, S.Y. Optical, dielectric and thermal properties of nanoscaled films of polyalkylsilsesquioxane composites with star-shaped poly (ε-caprolactone) and their derived nanoporous analogues. *Polymer* **2003**, *44*, 2519–2527. [[CrossRef](#)]
38. Hu, Q.; Marand, E. In situ formation of nanosized TiO<sub>2</sub> domains within poly (amide–imide) by a sol-gel process. *Polymer* **1999**, *40*, 4833–4843. [[CrossRef](#)]

39. Zhang, J.; Wang, B.-J.; Ju, X.; Liu, T.; Hu, T.-D. New observations on the optical properties of PPV/TiO<sub>2</sub> nanocomposites. *Polymer* **2001**, *42*, 3697–3702. [[CrossRef](#)]
40. Gupta, K.K.; Kundan, A.; Mishra, P.K.; Srivastava, P.; Mohanty, S.; Singh, N.K.; Mishrad, A.P.; Maiti, P. Polycaprolactone composites with TiO<sub>2</sub> for potential nanobiomaterials: tunable properties using different phases. *Phys. Chem. Chem. Phys.* **2012**, *14*, 12844–12853. [[CrossRef](#)] [[PubMed](#)]
41. Thamaphat, K.; Limsuwan, P.; Ngotawornchai, B. Phase characterization of TiO<sub>2</sub> powder XRD and TEM. *Nat. Sci.* **2008**, *42*, 357–361.
42. Scherrer, P. Bestimmung der inneren struktur und der gröÙe von kolloidteilchen mittels röntgenstrahlen. In *Kolloidchemie ein lehrbuch*; Springer: Berlin/Heidelberg, Germany, 1912; pp. 387–409.
43. Patterson, A. The scherrer formula for x-ray particle size determination. *Phys. Rev.* **1939**, *56*, 978–982. [[CrossRef](#)]
44. Ren, Y.; Wei, Z.; Wu, T.; Bian, Y.; Leng, X.; Zhou, C.; Li, Y. Synthesis of highly branched poly ( $\delta$ -valerolactone) s: A comparative study between comb and linear analogues. *RSC Adv.* **2016**, *6*, 45791–45801. [[CrossRef](#)]
45. Furuhashi, Y.; Sikorski, P.; Atkins, E.; Iwata, T.; Doi, Y. Structure and morphology of the aliphatic polyester poly ( $\delta$ -valerolactone) in solution-grown, chain-folded lamellar crystals. *J. Polym. Sci. Part B Polym. Phys.* **2001**, *39*, 2622–2634. [[CrossRef](#)]
46. Kiran, A.; Kumar, T.; Sanghavi, R.; Doble, M.; Ramakrishna, S. Antibacterial and bioactive surface modifications of titanium implants by PCL/TiO<sub>2</sub> nanocomposite coatings. *Nanomaterials* **2018**, *8*, 860. [[CrossRef](#)] [[PubMed](#)]
47. Coates, J. Interpretation of infrared spectra, a practical approach. *Encycl. Anal. Chem.* **2000**, *12*, 10815–10837.
48. Aubin, M.; Prud'homme, R.E. Preparation and properties of poly (valerolactone). *Polymer* **1981**, *22*, 1223–1226. [[CrossRef](#)]
49. Kasyapi, N.; Bhowmick, A.K. Nanolamellar triblock of poly-d, l-lactide– $\delta$ -valerolactone–d, l-lactide with tuneable glass transition temperature and crystallinity for use as a drug-delivery vesicle. *RSC Adv.* **2014**, *4*, 27439–27451. [[CrossRef](#)]
50. He, D.; Hu, Y.; Tao, J.; Zheng, X.; Liu, H.; Jing, G.; Lu, H.; Guan, H.; Yu, J.; Zhang, J. Micro fiber with cladding of titanium dioxide (TiO<sub>2</sub>) nanoparticles and its violet light sensing. *Opt. Mater. Express* **2017**, *7*, 264–272. [[CrossRef](#)]
51. Oyama, H.T. Super-tough poly (lactic acid) materials: Reactive blending with ethylene copolymer. *Polymer* **2009**, *50*, 747–751. [[CrossRef](#)]
52. Liu, H.; Chen, F.; Liu, B.; Estep, G.; Zhang, J. Super toughened poly (lactic acid) ternary blends by simultaneous dynamic vulcanization and interfacial compatibilization. *Macromolecules* **2010**, *43*, 6058–6066. [[CrossRef](#)]
53. Liu, H.; Song, W.; Chen, F.; Guo, L.; Zhang, J. Interaction of microstructure and interfacial adhesion on impact performance of polylactide (pla) ternary blends. *Macromolecules* **2011**, *44*, 1513–1522. [[CrossRef](#)]
54. Wunderlich, B. *Thermal Analysis of Polymeric Materials*; Springer: Berlin/Heidelberg, Germany, 2005.
55. Jiang, S.; Ji, X.; An, L.; Jiang, B. Crystallization behavior of PCL in hybrid confined environment. *Polymer* **2001**, *42*, 3901–3907. [[CrossRef](#)]
56. Wang, G.; Chen, G.; Wei, Z.; Yu, T.; Liu, L.; Wang, P.; Chang, Y.; Qi, M. A Comparative Study of TiO<sub>2</sub> and Surface-Treated TiO<sub>2</sub> Nanoparticles on Thermal and Mechanical Properties of Poly( $\epsilon$ -caprolactone) Nanocomposites. *J. Appl. Polym. Sci.* **2012**. [[CrossRef](#)]
57. Jeziorny, A. Parameters characterizing the kinetics of the non-isothermal crystallization of poly (ethylene terephthalate) determined by DSC. *Polymer* **1978**, *19*, 1142–1144. [[CrossRef](#)]
58. Ziabicki, A. Crystallization of polymers in variable external conditions. *Colloid Polym. Sci.* **1996**, *274*, 705–716. [[CrossRef](#)]
59. Ozawa, T. Kinetics of non-isothermal crystallization. *Polymer* **1971**, *12*, 150–158. [[CrossRef](#)]
60. Avrami, M. Kinetics of phase change. I general theory. *J. Chem. Phys.* **1939**, *7*, 1103–1112. [[CrossRef](#)]
61. Francis, A. Non-isothermal crystallization kinetics of a blast furnace slag glass. *J. Am. Ceram. Soc.* **2005**, *88*, 1859–1863. [[CrossRef](#)]
62. Reinsch, V.E.; Rebenfeld, L. Crystallization processes in poly (ethylene terephthalate) as modified by polymer additives and fiber reinforcement. *J. Appl. Polym. Sci.* **1994**, *52*, 649–662. [[CrossRef](#)]
63. Di Lorenzo, M.; Silvestre, C. Non-isothermal crystallization of polymers. *Prog. Polym. Sci.* **1999**, *24*, 917–950. [[CrossRef](#)]

64. Desio, G.P.; Rebenfeld, L. Crystallization of fiber-reinforced poly (phenylene sulfide) composites. II. Modeling the crystallization kinetics. *J. Appl. Polym. Sci.* **1992**, *45*, 2005–2020. [[CrossRef](#)]
65. Wei, Z.; Wang, G.; Wang, P.; Liu, L.; Qi, M. Crystallization behavior of poly ( $\epsilon$ -caprolactone)/TiO<sub>2</sub> nanocomposites obtained by in situ polymerization. *Polym. Eng. Sci.* **2012**, *52*, 1047–1057. [[CrossRef](#)]
66. Kissinger, H.E. Variation of peak temperature with heating rate in differential thermal analysis. *J. Res. Natl. Bur. Stand.* **1956**, *57*, 217–221. [[CrossRef](#)]
67. Yang, Y.; Yu, Y.; Zhang, Y.; Liu, C.; Shi, W.; Li, Q. Lipase/esterase-catalyzed ring-opening polymerization: A green polyester synthesis technique. *Process. Biochem.* **2011**, *46*, 1900–1908. [[CrossRef](#)]
68. Vyazovkin, S.; Sbirrazzuoli, N. Isoconversional analysis of the nonisothermal crystallization of a polymer melt. *Macromol. Rapid Commun.* **2002**, *23*, 766–770. [[CrossRef](#)]
69. Friedman, H.L. Kinetics of thermal degradation of char-forming plastics from thermogravimetry. Application to a phenolic plastic. *J. Polym. Sci. Part C* **1964**, *6*, 183–195. [[CrossRef](#)]
70. Papageorgiou, G.Z.; Achilias, D.S.; Bikiaris, D.N.; Karayannidis, G.P. Crystallization kinetics and nucleation activity of filler in polypropylene/surface-treated sio2 nanocomposites. *Thermochim. Acta* **2005**, *427*, 117–128. [[CrossRef](#)]
71. Garozzo, D.; Giuffrida, M.; Montaudo, G. Primary thermal decomposition processes in aliphatic polyesters investigated by chemical ionization mass spectrometry. *Macromolecules* **1986**, *19*, 1643–1649. [[CrossRef](#)]
72. Kricheldorf, H.R.; Lüderwald, I. Strukturuntersuchung von polyestern durch direkten abbau im massenspektrometer, 3. Poly- $\beta$ -propiolacton, poly- $\beta$ -pivalolacton und poly- $\delta$ -valerolacton. *Die Makromol. Chemie Macromol. Chem. Phys.* **1978**, *179*, 421–427. [[CrossRef](#)]
73. Abe, H. Thermal degradation of environmentally degradable poly (hydroxyalkanoic acid) s. *Macromol. Biosci.* **2006**, *6*, 469–486. [[CrossRef](#)]
74. Broido, A. A simple, sensitive graphical method of treating thermogravimetric analysis data. *J. Polym. Sci. Part B Polym. Phys.* **1969**, *7*, 1761–1773. [[CrossRef](#)]



© 2018 by the authors. Licensee MDPI, Basel, Switzerland. This article is an open access article distributed under the terms and conditions of the Creative Commons Attribution (CC BY) license (<http://creativecommons.org/licenses/by/4.0/>).